Journal of Applied Polymer Science

Polymerization kinetics of styrene in isotactic polypropylene pellets and evolution of phase morphology during polymerization

Fang Chen, Zhao-Xia Guo, Jian Yu
Key Laboratory of Advanced Materials (MOE), Department of Chemical Engineering, Tsinghua University, Beijing, 100084, People's Republic of China
Correspondence to: Z.-X. Guo (E-mail: guozx@mail.tsinghua.edu.cn) and J. Yu (E-mail: yujian03@mail.tsinghua.edu.cn)

ABSTRACT: Polymerization kinetics of styrene (St) in commercially available isotactic polypropylene (iPP) pellets and the phase morphology evolution during polymerization are investigated. The polymerization rate of St in iPP pellets is slightly faster than in the corresponding bulk and suspension polymerizations carried out under similar reaction conditions due to the existence of two reaction sites: amorphous PP and polystyrene (PS), which are formed by polymerization-induced phase separation. Two mechanisms are proposed for the phase morphology evolution: nucleation and growth, and St-assisted coarsening of phase structure. During polymerization, the size of the dispersed PS particles increases with polymerization time no matter at which position of the pellet, but the increasing amplitude is much bigger at 200 μm distance to the edge than at the center due to much more significant occurrence of St-assisted coarsening of phase structure which is attributed to both high values of PS/PP and St/PP resulted from polymerization-induced diffusion of St. © 2016 Wiley Periodicals, Inc. J. Appl. Polym. Sci. **2016**, *133*, 43934.

KEYWORDS: blends; kinetics; morphology; polyolefins; radical polymerization

Received 23 February 2016; accepted 15 May 2016
DOI: 10.1002/app.43934

INTRODUCTION

As a type of nanomaterials,[1–5] nanoblends have received continuing attention since they are expected to have superior properties than the conventional micro-structured blends. A number of methodologies have been developed to make polymer nanoblends, including *in situ* polymerization and *in situ* compatibilization reactive extrusion,[6–8] supercritical CO_2-assisted infusion and subsequent polymerization,[9–11] high-shear processing,[12] conventional melt blending with small amount of minor component,[13] solid-state shear pulverization,[14] and so on.[15–26] Each approach involves its characteristic mechanism for the formation of nanoscaled dispersed phase.

In the *in situ* polymerization and *in situ* compatibilization reactive extrusion process,[6–8] a monomer (such as ε-caprolactam) is polymerized in a molten polymer matrix (such as PP) in the presence of a macro-activator (such as isocyanate-bearing PP). Different from conventional melt blending, phase morphology is formed by polymerization-induced phase separation rather than reducing the size of the dispersed phase, and nanodispersion is stabilized by the generation of a very high amount of graft copolymer acting as compatibilizer.

Using the fact that supercritical CO_2 is a good swelling agent and generally a poor solvent for most polymers,[9–11,27,28] various monomers (such as St and methyl methacrylate) and initiators (such as benzoyl peroxide [BPO] and azobisisobutyronitrile) have been diffused into the amorphous regions of a range of polymer matrices (such as PP, polyethy1ene, polychlorotrifluoroethylene, and polyformaldehyde), and polymer blends are formed upon polymerization. The size of the newly formed dispersed phase depends mainly on its content. When its content is not large, nanoblends are likely to form[11,28] because of the restriction arising from the crystalline regions of the matrix polymer.

High-shear processing is a simple mechanical blending technique without using compatibilizers.[12] The production of stable nanostructured blends such as poly(vinylidene fluoride) (PVDF)/nylon 11 relies on the unusually high-shear rates which result in improved miscibility of the two components through insertion of molecular chains of one component into the amorphous regions of the other component.

Conventional melt blending has been reported to be successful in preparing PVDF/acrylic rubber (ACM) nanoblends with very low ACM contents (<10 wt %),[13] because there is very good compatibility between PVDF and ACM resulted from the dipolar interaction between CF_2 groups of PVDF and ester groups of ACM, and also because the phase morphology can be fixed once phase separation occurs based on the fact that the phase

separation temperature is not far from the PVDF crystallization temperature.

In solid-state shear pulverization,[14] quasi-nanoscale dispersion of poly(methyl methacrylate) in PS matrix is achieved by repeated fragmentation and fusion steps within the pulverizer, and with the addition of a gradient copolymer, compatibilized nanoblends can be obtained without coarsening in subsequent high-temperature static annealing.

Despite of the existence of numerous preparation methods for nanoblends, effort is still needed to invent new methods and understand the formation mechanism, because each of the existing methods is only limited to one or few examples. Previously, our research group reported a method for the preparation of quasi-nanoblends in aqueous medium by diffusion and subsequent polymerization of St in commercially available iPP pellets which have quasi-spherical shape and a diameter around 4.5 mm.[29] PP is a widely used commodity plastic. Making PP-based nanoblends can provide high performance PP-based materials, enriching the variety of PP compounds. Compared to conventional melt blending, the advantages of the method include fine phase morphology, absence of polymer degradation and direct use of the products in plastic processing. The diffusion kinetics and characterizations of the blends were reported. The goal of this work is to understand the mechanism for the phase morphology evolution during polymerization and provide guidance for phase morphology control. Thus, the monomer conversion, molecular weight and diametrical distribution of PS, phase morphology and melting behavior of the blends as a function of time are investigated. The control of phase morphology is necessary in view of obtaining blend pellets with fine phase morphology in preparation for injection molding to produce useful PP/PS blend materials without macrophase-separation, unlike in the case of conventional melt mixing.

EXPERIMENTAL

Materials

Commercial grade iPP pellets, S1003, with a melt flow index of 3.2 g/10 min, density of 0.905 g/cm^3, and diameter of approximately 4.5 mm, were from Yanshan Petroleum and Chemical (Beijing, China). Polyvinyl alcohol (PVA) with a degree of polymerization of 1750 ± 50 and degree of alcoholysis of 88% was purchased from Beijing Organic Chemical Plant (Beijing, China). Styrene (St, from Tianjin DAMAO Chemical Plant, Tianjin, China) with a boiling point of 146 °C was purified by vacuum distillation. Benzoyl peroxide (BPO, from Tianjin Fuchen Chemical Reagents Factory, Tianjin, China) with a melting point of 103–105 °C was purified by recrystallization twice from chloroform/methanol. Chloroform, xylene, hydroquinone (HQ), and methanol were analytical grade and used as received. PS used for making calibration curve was purchased from Taita Chemical Co. Ltd (Taipei) and has a M_w of 2.3×10^5 g mol^{-1}.

Blend Synthesis

The diffusion and subsequent polymerization of St in iPP pellets were carried out using the previously reported "901" procedure,[29] where "90"means that the diffusion temperature is 90 °C and "1"means one pot procedure, except that the diffusion time is 2 h and BPO content is 1 wt % relative to St. Briefly, iPP pellets (20.0 g), pure water (52.5 mL), and aqueous PVA (7.5 mL, 0.8% in water) were added to a 250 mL flask equipped with a mechanical stirrer, mixed and then maintained at 90 °C. St (6 g, 30 wt % to iPP) was added to the mixture, and the diffusion of St into iPP pellets was carried out at 90 °C for 2 h. Then, BPO (60 mg) was added with the aid of 1 mL of chloroform. After a pre-determined time of polymerization (30, 45, 60, and 90 min), HQ was added and the mixture was stirred for 20 min at 90 °C to terminate polymerization. No HQ was added for the polymerization stopped at 180 min. After cooling to room temperature, the blend pellets were isolated by vacuum filtration, washed with water and dried.

Bulk and Suspension Polymerizations

Bulk and suspension polymerizations of St were carried out under the same reaction conditions to blend synthesis in keeping the same proportion of all the necessary reagents without iPP pellets.

Microscopic Fourier Transform Infrared Spectroscopy

Films with a thickness of 15 μm were cut through the center of iPP or iPP/PS blend pellets by a microtome (YD-1508R, Zhejiang Jinhua Yidi Medical Equipment Factory) and Microscopic Fourier transform infrared spectroscopy (Micro-FTIR) was performed with Thermo-Nicolet 6700 FT-IR and Nicolet Continuum FT-IR Microscope, with a microsampling area of 100×100 μm^2. FTIR spectra were recorded along diameter of single pellets. A_1/A_2 is defined as the ratio of the peak areas of the absorptions at 758 cm^{-1} and 1167 cm^{-1}, characteristics of the PS and Ipp, respectively, reflecting PS/PP at the measured position of the pellets.

For making the calibration curve, PP/PS blends with various compositions were prepared by melt mixing PP and PS using a Haake torque rheometer (Thermo Fisher Scientific, Co. Ltd, Germany), followed by melt-pressing into films, then FTIR spectra were recorded.

Measurements of PS Content, Monomer Conversion, and Grafting Ratio

PS content is defined as the weight ratio of PS contained by the blend pellets to the initial iPP pellets, that is, PS/PP, and measured by gravimetric method.

Monomer conversion is defined as the weight ratio of PS contained by iPP pellets after polymerization to St diffused into the pellets and measured by gravimetric method. The blend pellets after polymerization for 180 min were filtered and scrubbed with filter paper to remove water on the pellet surface, then weighed. The weight gain is regarded as that of total St diffused into the pellets. The weight of PS contained by iPP pellets after a predetermined time of polymerization is obtained after thorough drying of the blend pellets to remove unreacted St and is the weight gain compared to the original iPP pellets.

Grafting ratio is defined as the weight ratio of grafted PS to PP, and measured as follows. PP/PS blend pellets were dissolved in boiling xylene and then PP and PP-*g*-PS were precipitated with THF and carefully filtered. The precipitate (in the form of powder) was stirred in refluxing THF for 8 h to remove the remaining un-grafted PS if there is any, then cooled, carefully filtered and dried. A sample in the form of thin film for FTIR analysis

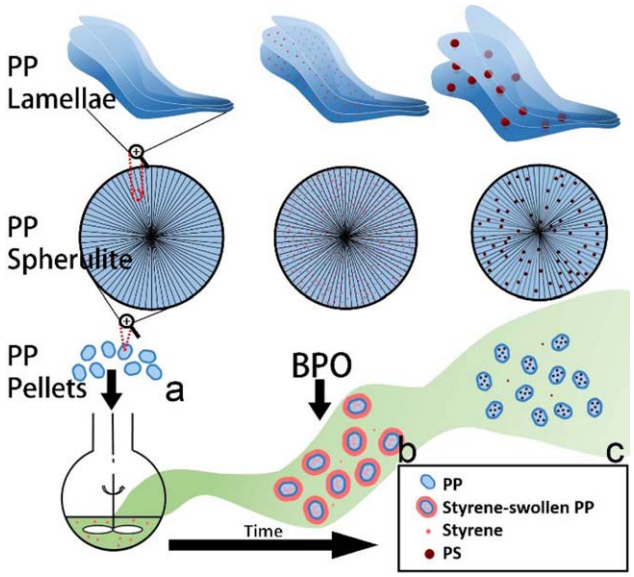

Figure 1. Illustration of the processes of diffusion and subsequent polymerization of St in iPP pellets. [Color figure can be viewed in the online issue, which is available at wileyonlinelibrary.com.]

was prepared by melt-pressing and analyzed to get an A_1/A_2 ratio. The process of refluxing in THF was repeated until A_1/A_2 ratio is constant. Grafting ratio is calculated according to the calibration curve. Grafting efficiency is defined as the weight ratio of grafted PS to total PS.

Field Emission Scanning Electron Microscopy

The morphology of the samples was visualized by JSM-7401 field emission scanning electron microscope (FESEM) at an accelerating voltage of 3 kV. Cross sections of single pellet for FESEM were obtained using the same cutting procedure as for FTIR, and then etched for 1 h with stirring in a mixture of water (5 g), sulfuric acid (6 g, 95%), orthophosphoric acid (9 g, 85%), and potassium permanganate (0.08 g) to remove the amorphous regions of iPP for better observation.[29] The samples were washed ultrasonically in water for 5 min and then in acetone for another 5 min before drying. Particle sizes were counted with the aid of the Smile View software.

Gel Permeation Chromatography

Pellets were hot pressed into a thin film of about 100 μm and then stirred in THF for 24 h to extract PS. The molecular weights (MWs) and distributions of PS were determined using a gel permeation chromatographic (GPC) apparatus operated using THF as the eluent (1 mL/min) at 25 °C and calibrated by means of polystyrene narrow standards.

Polarized Optical Microscopy

The crystalline morphology of the iPP pellet along the diameter direction was investigated by observing a film cut through the center of the iPP pellet with a Polarized Optical Microscope (POM; Olympus BX41P).

RESULTS AND DISCUSSION

Monomer Conversion and MW of PS versus Time

The processes of diffusion and subsequent polymerization of St in iPP pellets are illustrated in Figure 1. According to our previous work,[29] when iPP pellets are suspended in a mixture of water, St and PVA with stirring [Figure 1(a)], most of St is adsorbed on the surfaces of iPP pellets, and the rest of the St suspends in water as droplets. The role of PVA as a suspending agent is to prevent the occurrence of caking during subsequent polymerization. During 2 h of diffusion at 90 °C St diffuses in part into the amorphous regions of iPP pellets such as regions between lamellae and cores of the spherulites, due to more affinity to amorphous PP regions than to water, and there is some St left on the surfaces of iPP pellets because St is in excess [Figure 1(b)]. Upon the addition of BPO with the aid of chloroform, polymerization of St occurs. Although BPO is not water-soluble, it is soluble in styrene and can diffuse into iPP pellets along the diffusion paths of St to initiate polymerization of styrene inside iPP pellets. The polymerization was carried out at 90 °C to get a reasonable reaction rate because of the use of BPO as the initiator. As polymerization proceeds inside iPP pellets, the St on the surfaces of iPP pellets continues to diffuse into iPP pellets and polymerizes, and the St in the droplets migrates through the water to the surfaces of iPP pellets and then diffuses into iPP pellets. At the end of polymerization, PP/PS blend pellets with fine phase morphology are obtained [Figure 1(c)]. Inevitably, the St left in the droplets forms small PS particles in water, which can be removed by filtration. The St left on the surfaces of the pellets may also polymerize, however, the amount of PS on the surfaces of the pellets is greatly reduced when the amount of BPO (1 wt % to St in this work as compared to the previous 5 wt % to St) is reduced as shown by the Micro-FTIR spectra discussed later.

To investigate polymerization kinetics, an inhibitor is usually added to the reaction mixture at any pre-determined time to terminate polymerization. Therefore, the effectiveness of hydroquinone (HQ), a traditional inhibitor for radical chain polymerization, was investigated. Various amounts of HQ were added to the reaction mixture just after the addition of BPO, and PS

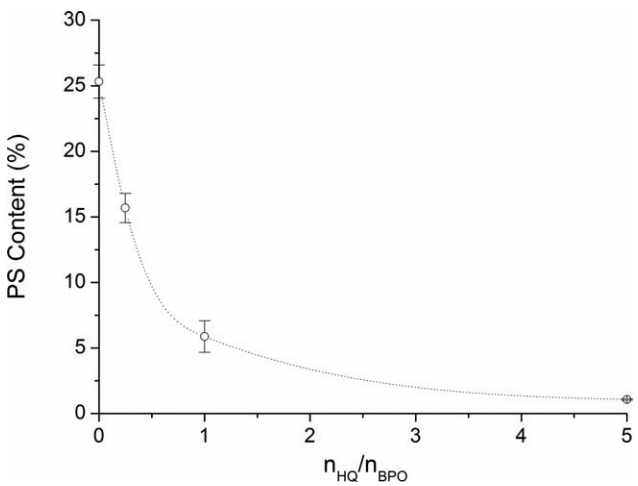

Figure 2. Curve of PS content versus n_{HQ}/n_{BPO}.

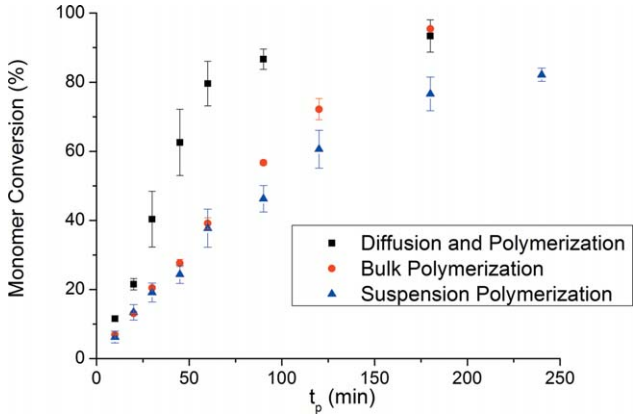

Figure 3. Curves of monomer conversion as a function of time for three different methods. [Color figure can be viewed in the online issue, which is available at wileyonlinelibrary.com.]

content after 3 h of polymerization as a function of the mol ratio of HQ/BPO (n_{HQ}/n_{BPO}) is shown in Figure 2. Clearly, PS content decreases with the increase in the amount of HQ, and when n_{HQ}/n_{BPO} is 5, polymerization almost stops. This indicates that HQ can partly diffuse into iPP pellets through the diffusion paths and can be used to terminate polymerization of St in iPP pellets despite of its hydrophilic nature. Therefore, in the current investigation on polymerization kinetics, a large excess amount of HQ ($n_{HQ}/n_{BPO} = 10$) was added to the reaction mixture at different polymerization times, and stirred for 20 min at 90 °C to allow HQ to diffuse into iPP pellets and terminate polymerization.

The curve of monomer conversion versus polymerization time (t_p) is shown in Figure 3 along with those of bulk and suspension polymerizations obtained under similar reaction conditions for comparison. In the first 60 min of polymerization, the rate for polymerization in iPP pellets is slightly higher than for the corresponding bulk and suspension polymerizations, the latter two having almost the same polymerization rate because each monomer droplet in a suspension polymerization behaves as a miniature bulk polymerization system. This indicates that the mechanism for polymerization of St in iPP pellets is more complicated than just being bulk polymerization in the free volume of the amorphous regions of iPP pellets.[30] It is not only a confined polymerization, but also accompanied by phase separation of PP and PS, which results in two different sites of polymerization (amorphous PP and PS phases).

At the very first beginning of polymerization, the movement of PS macroradicals is confined by the amorphous PP chains and the surrounded PP lamellae, polymerization rate is higher than bulk polymerization because of slow termination. The system is consisted of three components: PP, PS, and St. Referenced to the phase diagram reported for interpenetrating polymer networks,[31] shortly after polymerization is initiated phase separation occurs, forming spherical PS particles because PS and PP are immiscible. This can be referred to as "polymerization-induced phase separation." The St in the system is in part in PP, and in part in PS. The polymerization rate of St in PS is similar to that of bulk polymerization, while that in PP is higher than that of bulk polymerization due to the slower movement of PS macroradicals as a result of the confinement by the amorphous PP chains and the surrounded PP lamellae, and consequently the polymerization rate of St in iPP pellets is slightly higher than the cases of bulk and suspension polymerizations.

In order to prove the distribution of St in both PP and PS and find out the distribution ratio, the same amounts of neat iPP pellets and PP/PS (7:3) melt-blended pellets were put together as the matrices to carry out diffusion and polymerization of St. After 3 h of polymerization, the two types of pellets were separated and weighed. It was found that 38% of St distributes in neat iPP pellets and the other 62% in PP/PS melt-blended pellets, corresponding to a distribution of 3:1 in PS and PP. This indicates that the above-mentioned polymerization sites are reasonable.

At 180 min, the monomer conversions for polymerizations in pellets and in bulk are almost the same (93% and 95%), being higher than that of suspension polymerization (77%). This can be explained by their different kinetic behavior. The polymerization rate for polymerization in pellets is higher than those of the other two types of polymerizations during the first 60 min of reaction. Although the polymerization rate of bulk polymerization is the same as that of suspension polymerization during the first 60 min, it is higher than that of suspension polymerization after 60 min. Therefore, the monomer conversions at 180 min for polymerization in pellets and in bulk are both high, no much difference, while that of suspension polymerization is much lower due to slower polymerization rate.

Table I lists the weight-average molecular weights (M_w) and molar-mass dispersity of PS extracted by tetrahydrofuran from the reaction products obtained at different polymerization times. They do not vary much. The M_w is all around a hundred thousand with a molar-mass dispersity around 2, being in agreement with the general rule of free-radical chain polymerization without gel effect. It should be pointed out that PS cannot be completely extracted out from the products due to the occurrence of grafting. Free radicals can be generated on PP chains because of chain transfer from macroradicals or the initiator radicals, resulting in 1.2% of grafting (i.e., grafted PS/PP) which corresponds to a grafting efficiency of 4.5%. The GPC results are based on the extracted PS accounting for 95.5% of total PS.

Diametrical Distribution of PS versus Time

Figure 4 shows the diametrical distribution of PS obtained from Micro-FTIR spectra of the blend pellets at different polymerization times. The distance 0 is the center of the pellet. The ratio of the peak intensities at 758 and 1167 cm^{-1}, A_1/A_2, was taken

Table I. Molecular Weight and Polydispersity Data Obtained by GPC

t_p (min)	Polydispersity M_w/M_n	M_w (g mol^{-1})
30	2.58	1.0×10^5
45	1.91	1.3×10^5
60	1.72	1.0×10^5
90	1.89	0.8×10^5
180	1.89	0.9×10^5

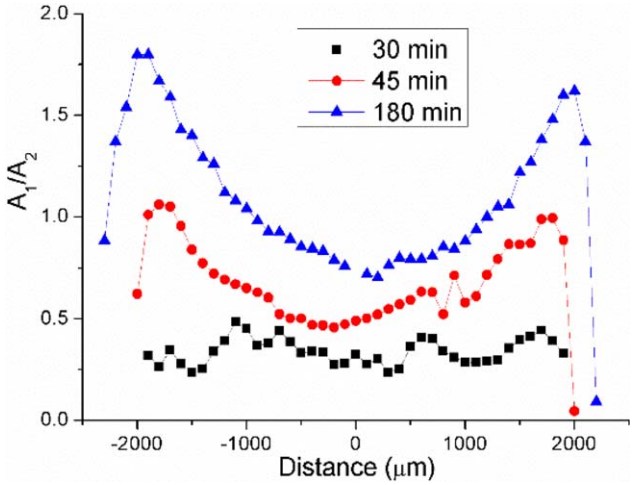

Figure 4. Diametrical distributions of PS at different polymerization times. (The distance 0 is the center of the pellet, and A_1/A_2 represents PS/PP). [Color figure can be viewed in the online issue, which is available at wileyonlinelibrary.com.]

to represent PS/PP. At 30 min of polymerization, the distribution of PS does not vary significantly from the edge to the center of the pellet, indicating almost homogeneous distribution of PS. At 180 min of polymerization, a typical saddle-shaped curve is obtained with the back at about 200 μm distance to the edge and the seat in the central region of the pellet. In fact, the saddle-shape has already started to develop at 45 min of polymerization.

The weight ratio of PS/PP at different positions of a pellet can be obtained from A_1/A_2 of Micro-FTIR spectra using a calibration curve shown in Figure 5. The curves of PS/PP at the center and 200 μm distance to the edge as a function of time are shown in Figure 6, along with PS content obtained by gravimetric method, representing average value of the whole pellet. At 30 min of polymerization, PS/PP at both the center and 200 μm distance to the edge are similar to the average value because of the homogeneous distribution of PS in the pellets. After 30 min of polymerization, PS/PP at the center are smaller than the average values, while that at 200 μm distance to the edge are

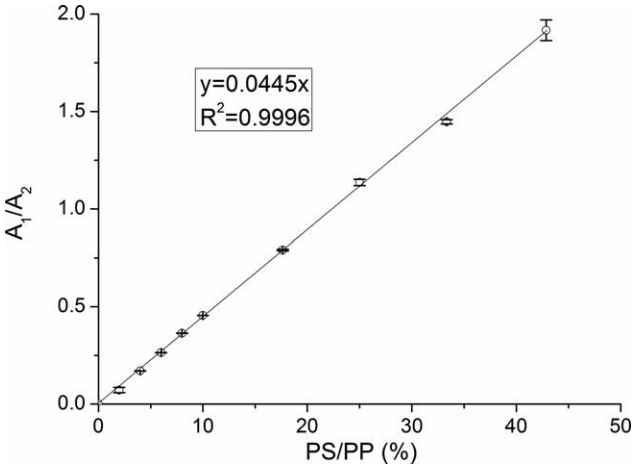

Figure 5. Calibration curve obtained from PP/PS films with different compositions.

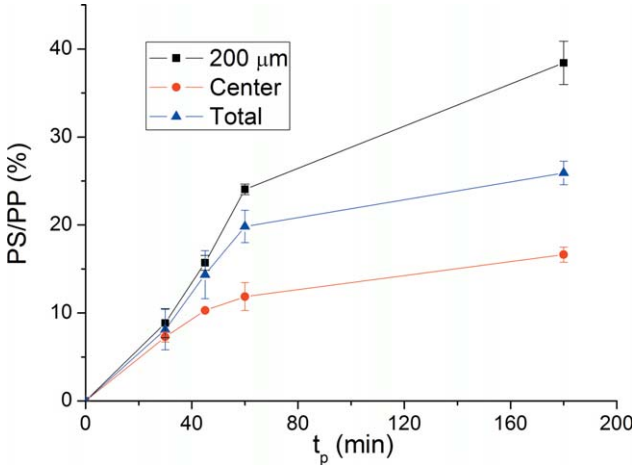

Figure 6. The weight ratio of PS/PP at different positions of a pellet as a function of polymerization time: (a) central area, (b) 200 μm to the edge, and (c) whole pellet. [Color figure can be viewed in the online issue, which is available at wileyonlinelibrary.com.]

higher. PS/PP at the center increases smoothly with time, while it increases much faster at 200 μm distance to the edge, especially during 30–60 min of polymerization. This indicates that further diffusion of St (also the BPO dissolved in it) into the pellets becomes obvious after 30 min of polymerization, and most of the newly coming St localizes at 200 μm distance to the edge of the pellets. The reasons for the diffusion of St into the pellets during polymerization are the increased PS content and reduced monomer concentration in the amorphous PP phase, both needing more monomer to get swelling equilibrium, and thus the phenomenon can be referred to as "polymerization-induced diffusion."

The position where St is enriched depends on many factors, such as the structural hierarchy[32–35] of the pellets, the amount of the initiator BPO, and St/PP value. The structural hierarchy of the pellets was clearly shown in the POM micrograph of a

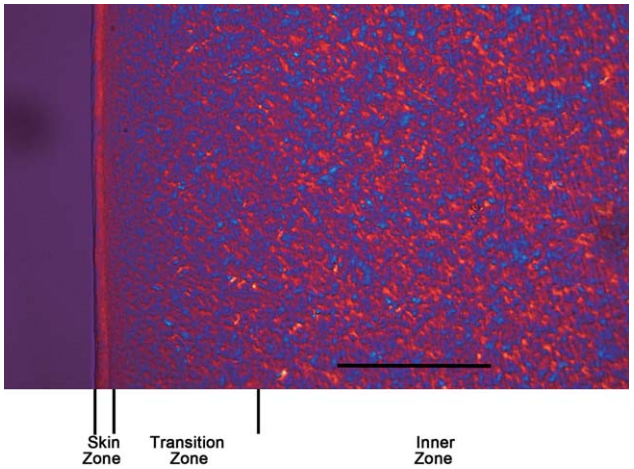

Figure 7. POM image showing skin zone, transition zone, and inner zone of an iPP pellet along the diameter direction. (Scale bar is 100 μm). [Color figure can be viewed in the online issue, which is available at wileyonlinelibrary.com.]

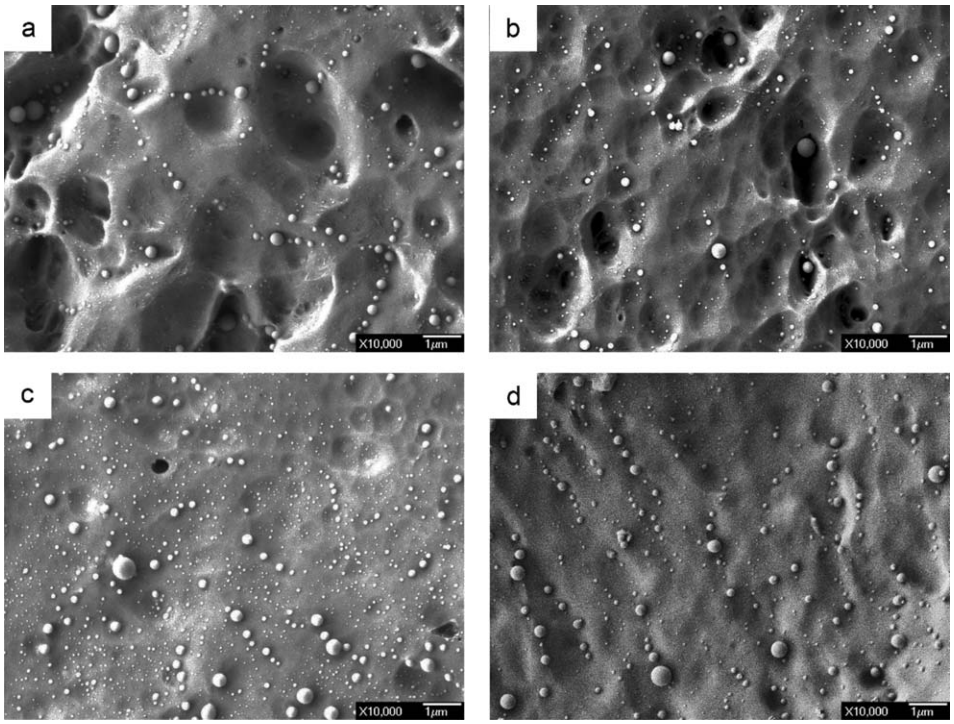

Figure 8. FESEM micrographs showing the dispersed PS phase in the central area of iPP pellets obtained by termination with HQ at different polymerization times: (a) 30 min, (b) 45 min, (c) 60 min, and (d) 180 min.

slice cut across the center of an iPP pellet (Figure 7). It consists of three distinct zones: skin zone, inner zone, and a transition zone in between, which have different crystal perfection because of different cooling rates during pelleting process of iPP. Even in the inner zone, the crystal perfection gradually increases from the boundary to the center, meaning the increasing diffusion resistance. In the current case the St-enriched position is 200 μm distance to the edge.

Evolution of Phase Morphology

In order to analyze the phase morphology evolution during polymerization of St, the phase morphology of the blend pellets obtained by termination with HQ at 90 °C for 20 min at different polymerization times was investigated by FESEM after removal of the amorphous region of iPP by manganic etching. FESEM micrographs of the products at two typical positions, the center and 200 μm distance to the edge, are shown in Figures 8 and 9.

The phase morphology at the center of the pellets (Figure 8) does not vary obviously from 30 to 180 min of polymerization. PS phase is observed as spherical particles, and the range of particle size is from a few nanometer to a few hundred nanometer with an average around 100 nm (Table II).

As mentioned earlier, phase separation occurs shortly after polymerization is initiated and the monomer inside the pellet is in part in amorphous PP, and in part in PS. On further polymerization, the PS chains formed by polymerization of the St in PP will deposit on PS particles, and the St in PS particles also polymerizes, both making PS particles grow. According to the nucleation and growth mechanism, the size of the dispersed PS phase should be controlled by the inter-lamella distance of iPP spherulites and the relative proportion of the two polymers (PS/PP). Because both the inter-lamella distance and PS/PP are very small, the PS particles formed by confined phase separation are very small, in nanometer to submicron sizes, much smaller than the size of the dispersed phase observed in the conventional melt blending. From 30 to 180 min of polymerization, the increase in PS particle size cannot be significantly observed, because PS/PP only increases slightly and the PS particles are in a wide range of sizes, although the average particle sizes at 60 min and 180 min are somewhat bigger than that obtained at 30 min (Table II).

The PS particle size at 200 μm distance to the edge of the pellets (Figure 9) varies significantly from 30 to 180 min of polymerization (Table II). At 30 min of polymerization, the average particle size is 86 nm, while at the end of polymerization (180 min), the average particle size is 263 nm, showing growth of PS particles. However, it was surprising to observe much bigger particle size (486 nm) for the sample obtained at 60 min. This indicates coarsening of the phase structure during termination with HQ at 90 °C for 20 min. Therefore, Figure 9(a–c) does not reflect the real phase morphology during polymerization.

It is noticed that at 60 min of polymerization not only PS/PP is much higher than at the center, but St/PP is also much higher because of the accumulation of newly coming St as mentioned earlier. The existence of large amount of St small molecules provides conditions for coarsening of the phase structure. At the end of polymerization (180 min), almost no St left, coarsening does not happen, that is why the apparent PS particle size at 200 μm distance to the edge listed in Table II decreases compared to that of 60 min. In order to prove this viewpoint, the

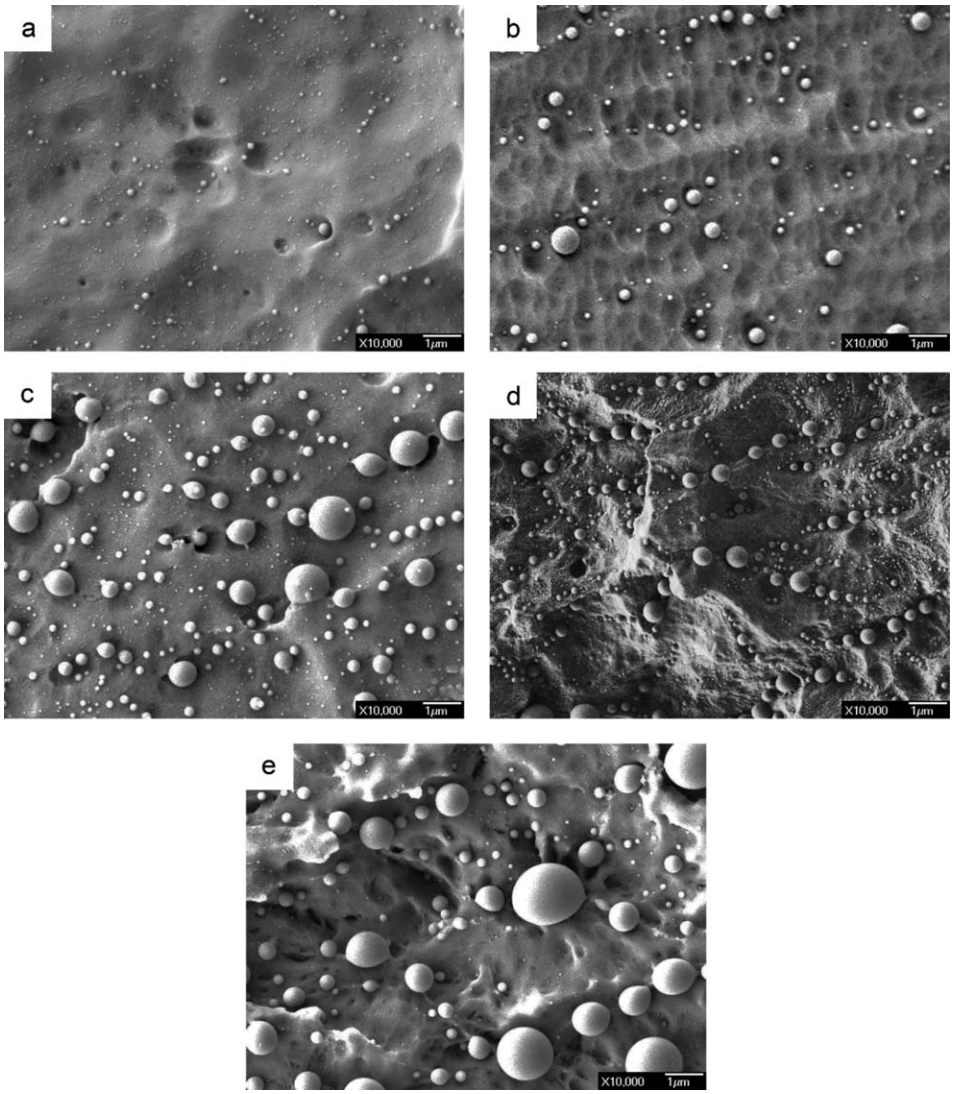

Figure 9. FESEM micrographs showing the dispersed PS phase at 200 μm to the edge of iPP pellets obtained by termination with HQ at different polymerization times: (a) 30 min, (b) 45 min, (c) 60 min, and (d) 180 min; and that showing coarsening of phase structure of sample d by treatment with water/xylene for 30 min at 90°C (e).

blend pellets obtained at the end of polymerization (180 min) were stirred in water/xylene (using the same proportion of water/St as in blend synthesis) at 90 °C for 30 min, and the average PS particle size was found to be 2.0 times bigger [i.e., 531 ± 373, Figure 9(e)], proving the occurrence of coarsening in the presence of xylene. As illustrated in Figure 10, there are two possible mechanisms for coarsening of the phase structure: coalescence and Ostwald ripening.[36–38] When xylene molecules enter into the inter-lamella regions of the pellets, the amorphous PP and PS particles are swollen by xylene and the inter-lamella distance increases [Figure 10(b,d)]. There are three components, amorphous PP, PS and xylene, in the regions, and xylene is acting as the solvent for amorphous PP and PS. Both PS and amorphous PP chain segments move because of the assistance of xylene which can considerably lower the T_gs of PS and PP. In the course of coalescence, the neighboring PS particles approach each other under the effect of van der Waals forces. If the diameter of the swollen PS particles is bigger than the inter-lamella distance, PS particles will be flattened into ellipsoidal shape. The development of the ellipsoidal PS particles along the lamella direction results in the occurrence of

Table II. Apparent Particle Sizes at the Center and 200 μm Distance to the Edge Obtained at Different Polymerization Times by Termination with HQ

t_p (min)	Particle size at center (nm)	Particle size at 200 μm area (nm)[a]
30	89 ± 57	86 ± 52
45	97 ± 70	204 ± 108
60	127 ± 103	486 ± 304
180	149 ± 106	263 ± 163

[a] The reported particle sizes of 30, 45, and 60 min do not reflect the real sizes during polymerization because of the occurrence of coarsening during treatment with HQ.

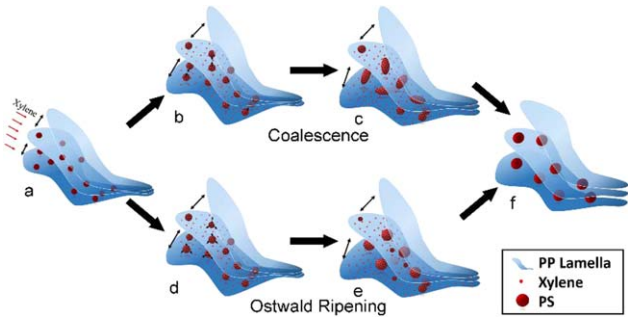

Figure 10. Illustration of xylene-assisted phase morphology evolution (amorphous PP chains are not shown due to difficulty of drawing). [Color figure can be viewed in the online issue, which is available at wileyonlinelibrary.com.]

coalescence [Figure 10(c)]. In the course of Ostwald ripening,[36] small PS particles dissolve and large PS particles grow [Figure 10(e)]. It is highly possible for some small PS particles to dissolve in xylene. Finally, spherical PS particles are obtained after drying, and the inter-lamella distance slightly retracts because of the evaporation of xylene small molecules [Figure 10(f)]. This model experiment confirms that swelling agent can indeed cause coarsening of the phase structure.

Based on the above discussion, the phase morphology evolution during polymerization and termination with HQ for the position of 200 μm distance to the edge of the pellets is proposed and illustrated in Figure 11. In the beginning of polymerization (less than 30 min), both PS/PP and St/PP are small, the coarsening of phase structure during termination with HQ is not obvious. In the middle stage of polymerization, such as 60 min, both PS/PP and St/PP are large, St-assisted coarsening of phase structure is significant during termination with HQ. If HQ is not added to the reaction mixture, in one hand polymerization of St will continue to proceed, resulting in bigger particle size according to the nucleation and growth mechanism; in the other hand St-assisted coarsening of phase structure also occurs. The two processes are in competition, but the results are alike. At the end of polymerization (180 min), almost no coarsening of phase structure occurs due to lack of St. From 30 to 180 min of polymerization PS/PP increases from 8 to 37%, corresponding to an increase of 63% in the diameter of PS particles, far less than the real increase (200%) observed in FESEM micrographs [Figure 9(a,d)]. This reveals that the phase morphology evolution for polymerization of St in iPP pellets not only involves the nucleation and growth mechanism, St-assisted coarsening of phase structure also plays an important role.

Table III. Results Obtained by DSC

t_p (min)	T_m (°C)	Melting enthalphy (J g^{-1})
0	165.7	103.6
30	164.2	109
45	164.2	104.9
60	164.2	101.2
90	164.4	106.2
180	164.5	102.6

In summary, during polymerization, the phase morphology evolution involves two mechanisms: nucleation and growth, and St-assisted coarsening of phase structure. There are two important parameters affecting the occurrence of the two mechanisms and phase morphology: PS/PP and St/PP. During polymerization, at the center of the pellet these two parameters are both small, neither of the two mechanisms occurs in a great extent, and, therefore, the size of the dispersed phase is not big; at 200 μm distance to the edge of the pellets both PS/PP and St/PP are much bigger than at the center after 30 min of polymerization, both mechanisms occur in a much greater extent and thus the PS particle size is much larger than at the center. During polymerization, the size of PS particles increases with polymerization time, no matter which position, the difference is much bigger increasing amplitude at 200 μm distance to the edge of the pellets than at the center due to mainly significant occurrence of St-assisted coarsening of phase structure.

Unchanged Crystallinity of iPP

The melting behavior of the blend pellets obtained at different polymerization times was characterized by DSC in order to evaluate if diffusion and subsequent polymerization of St affect the crystalline portions of iPP pellets. The data are listed in

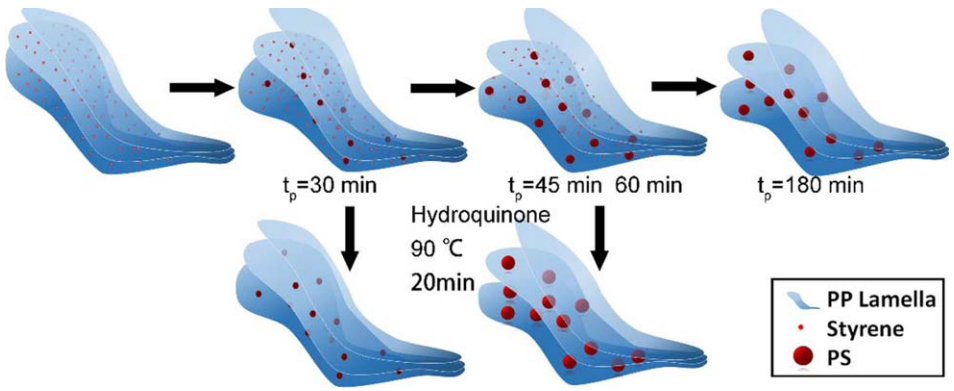

Figure 11. Illustration of phase morphology evolution during polymerization and termination by HQ at 200 μm to the edge of the pellets (amorphous PP chains are not shown in the Figure due to difficulty of drawing). [Color figure can be viewed in the online issue, which is available at wileyonlinelibrary.com.]

Table III. Clearly, both melting temperature (T_m) and enthalpy of melting (ΔH_m) of PP have no obvious change as a function of polymerization time, confirming the occurrence of St diffusion and polymerization only in the amorphous regions of iPP pellets. This is in agreement with the literature reports on supercritical carbon dioxide-assisted diffusion and subsequent polymerization of St in PP films.[9–11]

CONCLUSIONS

The polymerization rate of St in iPP pellets is slightly higher than in the corresponding bulk and suspension polymerizations, because the polymerization takes place in two sites: amorphous PP and PS phases, which are formed by polymerization-induced phase separation. Polymerization in the PS phase resembles bulk polymerization, while that in PP is faster due to slow termination resulted from slow movement of PS macroradicals which is confined by the amorphous PP chains. The weight-average molecular weight (M_w) and polydispersity of PS do not vary much as a function of time. The M_w is all around a hundred thousand with a polydispersity around 2. Almost homogeneous diametrical distribution of PS is observed in the first 30 min of polymerization. At the end of polymerization (180 min), a typical saddle-shaped distribution is observed with two maxima at about 200 μm distance to the edge where St from polymerization-induced diffusion is enriched due to the structural hierarchy of iPP pellets. The phase morphology evolution during polymerization involves two mechanisms: nucleation and growth, and St-assisted coarsening of phase structure. PS/PP and St/PP are two important parameters affecting the occurrence of the two mechanisms and phase morphology.

Taking the center and 200 μm distance to the edge as two typical positions of the pellets for comparison, during the first 30 min of polymerization, both PS/PP and PS particle size are similar, and the phase morphology evolution mainly involves nucleation and growth mechanism for the two positions. After 30 min of polymerization, both PS/PP and PS particle size increase smoothly with time at the center, and much faster at 200 μm distance to the edge. From 30 to 180 min of polymerization, PS/PP changes from 7 to 15% at the center and from 7 to 35% at 200 μm distance to the edge, and PS particle size increases from 89 to 149 nm at the center and from 86 to 263 nm at 200 μm distance to the edge. St-assisted coarsening of phase structure occurs much more significantly at 200 μm distance to the edge.

This work has identified that the polymerization-induced diffusion of St during polymerization is the main reason for the uneven diametrical distribution of PS and PS particle size, providing good guidance for the control of phase morphology in the preparation of PP/PS quasi-nanoblend pellets suitable for low-shear processing. The morphology and mechanical properties of the PP/PS blends after injection molding will be reported in a following paper.

ACKNOWLEDGMENTS

This work was supported by the National Natural Science Foundation of China (No. 51173095).

REFERENCES

1. Campos, J. M.; Lourenco, J. P.; Cramail, H.; Ribeiro, M. R. *Prog. Polym. Sci.* **2012**, *37*, 1764.
2. Lee, Y. C.; Lee, K.; Oh, Y. K. *Bioresour. Technol.* **2015**, *184*, 63.
3. Fang, R. H.; Luk, B. T.; Hu, C. M.; Zhang, L. *Adv. Drug. Deliv. Rev.* **2015**, DOI: 10.1016/j.addr.2015.04.001.
4. Kibria, M. A.; Anisur, M. R.; Mahfuz, M. H.; Saidur, R.; Metselaar, I. H. S. C. *Energy Convers. Manage.* **2015**, *95*, 69.
5. Nasir, A.; Kausar, A.; Younus, A. *Polym.-Plast. Technol. Eng.* **2015**, *54*, 325.
6. Hu, G. H.; Cartier, H.; Plummer, C. *Macromolecules* **1999**, *32*, 4713.
7. Ji, Y. L.; Li, W. G.; Ma, J. H.; Liang, B. R. *Macromol. Rapid Commun.* **2005**, *26*, 116.
8. Hou, L. L.; Liu, H. Z.; Yang, G. S.; Hou, L. L.; Liu, H. Z.; Yang, G. S. *Polym. Eng. Sci.* **2006**, *46*, 1196.
9. Kung, E.; Lesser, A. J.; McCarthy, T. *J. Macromolecules* **1998**, *31*, 4160.
10. Zhu, R.; Hoshi, T.; Chishima, Y.; Muroga, Y.; Hagiwara, T.; Yano, S.; Sawaguchi, T. *Macromolecules* **2011**, *44*, 6103.
11. Liu, Z. M.; Dong, Z. X.; Han, B. X.; Wang, J. Q.; He, J.; Yang, G. Y. *Chem. Mater.* **2002**, *14*, 4619.
12. Shimizu, H.; Li, Y. J.; Kaito, A.; Sano, H. *Macromolecules* **2005**, *38*, 7880.
13. Li, Y. J.; Wakura, Y.; Zhao, L.; Shimizu, H. *Macromolecules* **2008**, *41*, 3120.
14. Tao, Y.; Kim, J.; Torkelson, J. M. *Polymer* **2006**, *47*, 6773.
15. Ibuki, J.; Charoensirisomboon, P.; Chiba, T.; Ougizawa, T.; Inoue, T.; Weber, M.; Koch, E. *Polymer* **1999**, *40*, 647.
16. Bhardwaj, R.; Mohanty, A. K. *Biomacromolecules* **2007**, *8*, 2476.
17. Chan, S. H.; Lin, Y. Y.; Ting, C. *Macromolecules* **2003**, *36*, 8910.
18. Koulic, C.; Jerome, R. *Macromolecules* **2004**, *37*, 888.
19. Walther, A.; Matussek, K.; Muller, A. H. E. *ACS Nano* **2008**, *2*, 1167.
20. Kausar, A.; Zulfiqar, S.; Sarwar, M. I. *Polym. Adv. Technol.* **2014**, *25*, 196.
21. Kausar, A.; Zulfiqar, S.; Sarwar, M. I. *J. Appl. Polym. Sci.* **2014**, *131*, DOI: 10.1002/app.39954.
22. Costa, L. C.; Neto, A. T.; Hage, E. *Express Polym. Lett.* **2014**, *8*, 164.
23. Seo, Y. H.; Cho, M. J.; Cheong, O. J.; Jang, W. D.; Ohulchanskyy, T. Y.; Lee, S.; Choi, D. H.; Prasad, P. N.; Kim, S. *Biomaterials* **2015**, *39*, 225.
24. Zavareh, S.; Samandari, G. *Polym. Eng. Sci.* **2014**, *54*, 1833.
25. Bharatwaj, B.; Dimovski, R.; Conti, D. S.; da Rocha, S. R. P. *AAPS J.* **2014**, *16*, 522.
26. Kotal, M.; Srivastava, S. K.; Paramanik, B. *J. Phys. Chem. C* **2011**, *115*, 1496.
27. Watkins, J. J.; Mccarthy, T. *J. Macromolecules* **1994**, *27*, 4845.
28. Watkins, J. J.; Mccarthy, T. *J. Macromolecules* **1995**, *28*, 4067.
29. Yao, X. R.; Yu, J.; Guo, Z. X. *Polymer* **2011**, *52*, 667.
30. Yao, X. R.; Chen, F.; Guo, Z. X.; Yu, J. *Chin. Chem. Lett.* **2012**, *23*, 753.

31. Sperling, L. H. In Interpenetrating Polymer Networks: An Overview; Klempner, D.; Sperling, L. H.; Utracki, L. A., Eds.; American Chemical Society: Washington, DC, **1994**; Vol. *239*, pp 3–38.
32. Menges, G.; Wubken, G.; Horn, B. *Colloid. Polym. Sci.* **1976**, *254*, 267.
33. Zheng, G. O.; Yang, W.; Yang, M. B.; Chen, J. B.; Li, Q.; Shen, C. Y. *Polym. Eng. Sci.* **2008**, *48*, 976.
34. Wang, K.; Chen, F.; Li, Z. M.; Fu, Q. *Prog. Polym. Sci.* **2014**, *39*, 891.
35. Viana, J. C. *Polymer* **2004**, *45*, 993.
36. Crist, B.; Nesarikar, A. R. *Macromolecules* **1995**, *28*, 890.
37. Fortelny, I.; Zivny, A.; Juza, J. *J. Polym. Sci. Part B: Polym. Phys.* **1999**, *37*, 181.
38. Stachurski, Z. H.; Edward, G. H.; Yin, M.; Long, Y. *Macromolecules* **1996**, *29*, 2131.